*Human Molecular Genetics, 2011, Vol. 20, No. 11* **2091–2102**
*doi:10.1093/hmg/ddr091*
*Advance Access published on March 4, 2011*

# Parkin mediates beclin-dependent autophagic clearance of defective mitochondria and ubiquitinated Aβ in AD models

**Preeti J. Khandelwal[1], Alexander M. Herman[2], Hyang-Sook Hoe[1], G. William Rebeck[1] and Charbel E.-H. Moussa[1,2,*]**

[1]Department of Neuroscience and [2]Department of Biochemistry Molecular and Cell Biology, Georgetown University Medical Center, Washington, DC 20007, USA

Received December 3, 2010; Revised February 21, 2011; Accepted February 28, 2011

**Intraneuronal amyloid-β (Aβ) may contribute to extracellular plaque deposition, the characteristic pathology of Alzheimer's disease (AD). The E3-ubiquitin ligase parkin ubiquitinates intracellular proteins and induces mitophagy. We previously demonstrated that parkin reduces Aβ levels in lentiviral models of intracellular Aβ. Here we used a triple transgenic AD (3xTg-AD) mouse, which over-expresses $APP_{Swe}$, $Tau_{P301L}$ and harbor the $PS1_{M146V}$ knock-in mutation and found that lentiviral parkin ubiquitinated intracellular Aβ *in vivo*, stimulated beclin-dependent molecular cascade of autophagy and facilitated clearance of vesicles containing debris and defective mitochondria. Parkin expression decreased intracellular Aβ levels and extracellular plaque deposition. Parkin expression also attenuated caspase activity, prevented mitochondrial dysfunction and oxidative stress and restored neurotransmitter synthesis. Restoration of glutamate synthesis, which was independent of glial-neuronal recycling, depended on mitochondrial activity and led to an increase in γ-amino butyric acid levels. These data indicate that parkin may be used as an alternative strategy to reduce Aβ levels and enhance autophagic clearance of Aβ-induced defects in AD. Parkin-mediated clearance of ubiquitinated Aβ may act in parallel with autophagy to clear molecular debris and defective mitochondria and restore neurotransmitter balance.**

## INTRODUCTION

Alzheimer's disease (AD) is an aging disorder, characterized by extracellular deposits known as amyloid plaques, which consist of aggregates of amyloid-β (Aβ) peptide (1,2). Proteolytic cleavage of amyloid precursor protein (APP) by the β-site APP cleaving enzyme (BACE1) near the C-terminus results in the formation of APP C-terminal fragment (CTFβ) C99. Subsequent cleavage of CTFβ by γ-secretase generates Aβ of 40 ($Aβ_{40}$) or 42 ($Aβ_{42}$) residues (3), which is the predominant isoform in plaques (4). Alternatively, APP cleavage by α-secretase to generate APP (CTFα) C83 occurs within the Aβ region, precluding its formation (5,6). Intracellular accumulation of Aβ in transgenic animals and brains of human patients with AD and Down's syndrome (7) provides evidence for the presence of intracellular Aβ within neurons. $Aβ_{42}$ is found in multivesicular bodies of neurons in the human brain, where it is associated with synaptic pathology (8). In triple transgenic AD (3xTg-AD) mice, which overexpress $APP_{Swe}$, $Tau_{P301L}$ and harbor $PS1_{M146V}$ knock-in mutation, soluble and oligomeric Aβ accumulate within neuronal cell bodies, but the intraneuronal pool decreases when extracellular plaques appear (9), consistent with the data from human brain tissue (10–12). Taken together, these data suggest that in early stage AD the human brain might have abundant intraneuronal Aβ, which then becomes extracellular as the disease progresses and neurons die.

Mutations in the gene coding for the E3-ubiquitin (Ub) ligase parkin have been associated with autosomal recessive forms of Parkinson's disease (PD) (13). Parkin is ubiquitously expressed in neurons and astrocytes (14,15), and glial dysfunction is

*To whom correspondence should be addressed at: Department of Neuroscience and Department of Biochemistry, Molecular and Cell Biology, Georgetown University School of Medicine, 3970 Reservoir Rd, NW, TRB, Room WP09B, Washington, DC 20057. Tel: +1 2026877328; Fax: +1 2026870617; Email: cem46@georgetown.edu

observed in parkin-null mice (16). Parkin acts in parallel with the PTEN-induced putative kinase 1 to mediate selective autophagy of defective mitochondria (17–20). Upon mitochondrial membrane depolarization, parkin ubiquitinates mitochondrial proteins, induces microtubule-associated protein light chain 3 (LC3) and forms autophagosomes (21–25), suggesting a link between parkin and autophagic clearance. In mammalian cells, ubiquitination facilitates selective autophagy of diverse substrates, including protein aggregates, ribosomes, peroxisomes and pathogens (22,26). This process may contribute to the removal of damaged organelles or protein aggregates in neurodegenerative diseases.

In AD, Aβ and Tau aggregation are associated with mitochondrial damage, oxidative stress as well as structural and functional alterations of neurons (27–30). Parkin can be used as an alternative strategy to stimulate autophagic clearance of cellular and molecular debris associated with accumulation of amyloid proteins. To determine whether parkin could promote Aβ clearance, we injected 3xTg-AD mice with lentiviral parkin. We examined the effects of parkin on possible Aβ clearance mechanisms, including ubiquitination and autophagy. We also investigated the effects of Aβ clearance on mitochondrial tricarboxylic acid (TCA) cycle and neurotransmitter synthesis, including glutamate and γ-amino butyric acid (GABA). Understanding the effects of parkin-mediated attenuation of Aβ-induced mitochondrial dysfunction, oxidative stress and alteration of neurotransmitter levels may help clarify the role of intraneuronal Aβ in disease progression.

## RESULTS

### Western blot, enzyme-linked immunosorbent assay and mass spectroscopy show that parkin expression decreases ubiquitinated Aβ levels in 3xTg-AD mice

To examine the effects of the E3-Ub ligase parkin on Aβ levels, we used 3xTg-AD mice and injected lentiviral parkin in the right (ipsilateral) hippocampus and compared the contralateral left hemisphere. Animals ($n = 23$) were injected at 10–13 months of age and sacrificed 3 months post-injection (13–16 months), the hemispheres were separated and comparison was made between detergent and formic acid (FA) extracted right and left hemispheres. Staining with parkin antibody showed endogenous parkin levels (Fig. 1A) in cortical sections of 3xTg-AD mice. Injection with lentiviral parkin into the right hemisphere revealed an increase in parkin staining (Fig. 1B), and higher magnification showed intraneuronal parkin expression (Fig. 1C). Because expression was observed throughout the right-injected hemisphere (data not shown), we averaged stereological counting of parkin-positive cells in 10 different areas in the cortex, hippocampus and entorhinal cortex ($n = 7$). Stereological counting revealed 52% increase in parkin-injected hemispheres ($P < 0.05$) compared with the contralateral un-injected or LacZ injected hemispheres (Fig. 1D). Western blot analysis of brain lysates showed a significant increase ($P < 0.05$, $n = 8$) in parkin levels (48%) in the ipsilateral hemisphere (Fig. 1E and F). No significant changes were observed in holoAPP, secreted APPα and APPβ (Fig. 1E and F). A significant decrease (30%) in the levels of CTFs was observed in the parkin-injected hemisphere (Fig. 1E and F). No changes were observed in the levels of Tau protein between ispilateral and contralateral hemispheres in these animals (data not shown). We analyzed Aβ to determine whether the reduction in CTFs correlated with a reduction in Aβ levels. Specific human $Aβ_{42}$ and $Aβ_{40}$ enzyme-linked immunosorbent assay (ELISA) showed that parkin expression significantly decreased the detergent-extracted levels of $Aβ_{42}$ (40%) and $Aβ_{40}$ (29%) compared with the contralateral side (Fig. 1G). Parkin also significantly ($P < 0.05$, $n = 8$) decreased the FA-extracted levels of $Aβ_{42}$ (25%) and $Aβ_{40}$ (23%). These data demonstrate that parkin can reduce the levels of intracellular APP fragments, including Aβ.

We previously showed that parkin can ubiquitinate and clear intracellular $Aβ_{42}$ in a gene transfer animal model (31), and stimulate proteasomal activity to clear amyloid in cell culture (32). To determine the mechanisms by which parkin reduces Aβ levels in 3xTg-AD mice, we immunoprecipitated brain lysates with Ub antibodies (Fig. 1H) and performed western blot analyses. The anti-Aβ (6E10) antibody revealed a ∼14 kDa band, and a >100 kDa band in the parkin-injected side, but not the contralateral side. The anti-Ub antibody showed a smear of ubiquitinated proteins, which was more extensive in the parkin-injected hemisphere. The parkin-injected hemisphere demonstrated a 14 kDa Ub-positive band. We isolated the 14 kDa band and performed MALDI-TOF mass spectroscopy (Fig. 1I and J) to identify proteins in this band. Both Aβ and Ub fragments were sequenced (Fig. 1I and J) and identified in the 14 kDa band in parkin-injected brains. These data are consistent with our previous reports *in vitro* that parkin increases the ubiquitination of intracellular Aβ.

### Beclin-dependent molecular markers of autophagy and electron microscopy reveal parkin meditation of autophagic clearance in 3xTg-AD mice

We further investigated whether parkin also promotes autophagic clearance. Induction of autophagy involves several proteins, including beclin, the autophagy-related proteins (Atg) and LC3. Beclin was significantly (200%) increased ($P < 0.05$, $n = 8$) in parkin injected (Fig. 2A and B) compared with the contralateral hemispheres. Levels of Ub-like protein modification molecules were also significantly increased, including Atg7 (310%) and Atg12 (40%). Specific anti-LC3-B antibody showed a significant increase (50%) in LC3-B levels in the ipsilateral compared with the contralateral hemisphere (Fig. 2A and B). Thus, parkin expression increased several molecular markers of autophagy.

To further examine whether parkin mediates autophagy in 3xTg-AD mice, we used a different approach using scanning electron microscopy (EM) 1 month post-injection. EM scans of contralateral cortical sections ($n = 3$) showed cytosol containing vesicles filled with debris (Fig. 2C and D) and fragmented endoplasmic reticulum (ER). Higher magnification (Fig. 2E) revealed molecular debris and defective mitochondria within double-membrane vesicles, suggesting that the cell is attempting to remove damaged mitochondria and defective organelles. These data suggest accumulation of vesicles-loaded debris in the cytosol of 3xTg-AD brains,

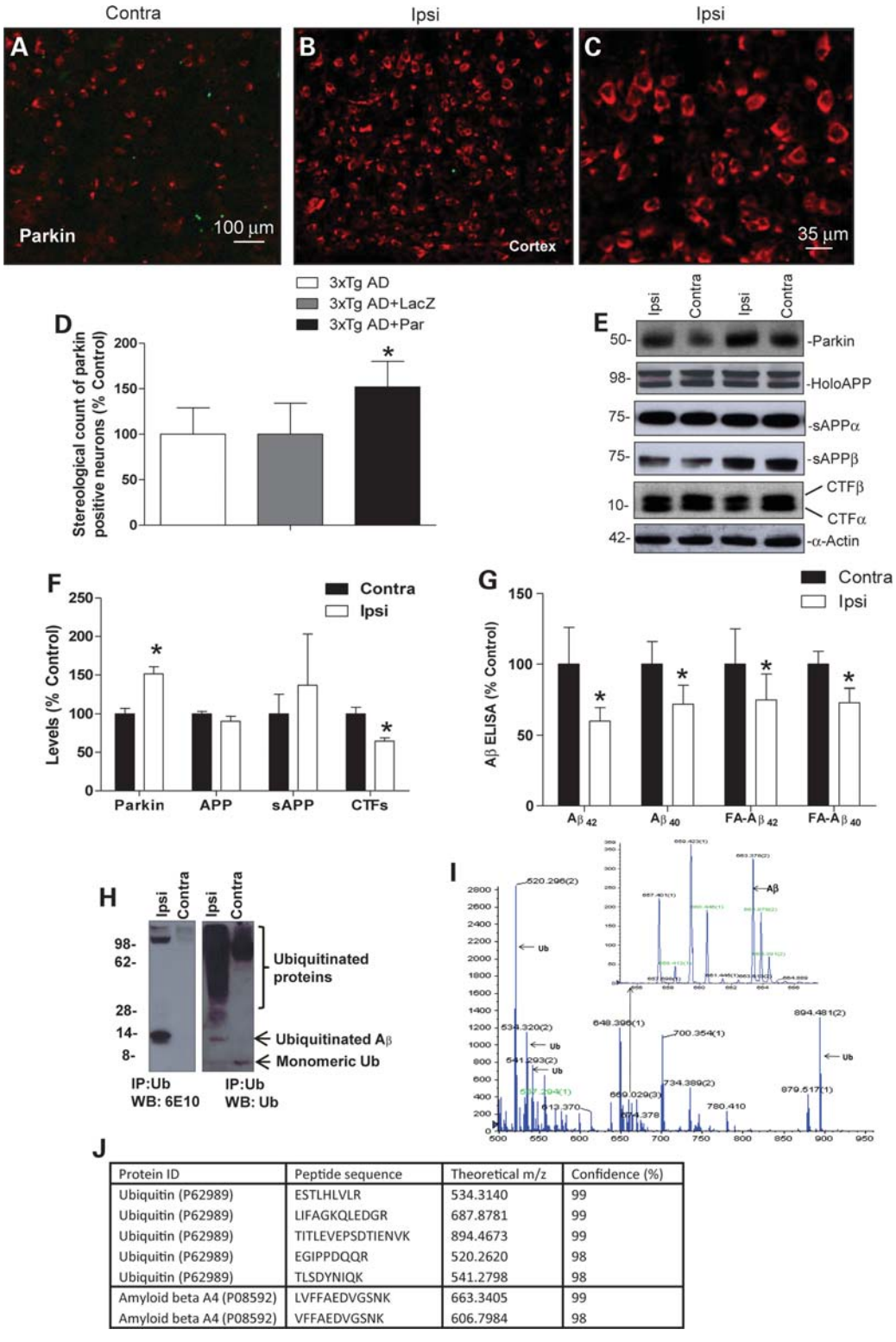


J

| Protein ID | Peptide sequence | Theoretical m/z | Confidence (%) |
|---|---|---|---|
| Ubiquitin (P62989) | ESTLHLVLR | 534.3140 | 99 |
| Ubiquitin (P62989) | LIFAGKQLEDGR | 687.8781 | 99 |
| Ubiquitin (P62989) | TITLEVEPSDTIENVK | 894.4673 | 99 |
| Ubiquitin (P62989) | EGIPPDQQR | 520.2620 | 98 |
| Ubiquitin (P62989) | TLSDYNIQK | 541.2798 | 98 |
| Amyloid beta A4 (P08592) | LVFFAEDVGSNK | 663.3405 | 99 |
| Amyloid beta A4 (P08592) | VFFAEDVGSNK | 606.7984 | 98 |

**Figure 1.** Western blot, ELISA and mass spectroscopy show parkin decrease of ubiquitinated Aβ levels in 3xTg-AD mice. Immunhistochemistry of 20 µm thick cortical brain sections of (**A**) contralateral and (**B**) parkin-injected (ipsilateral) hemispheres from 3xTg-AD mice. (**C**) Higher magnification of parkin stained cells in the cortex. (**D**) Stereological counting of parkin-positive cells in the ipsilateral compared with contralateral hemispheres. (**E**) Western blot analysis and (**F**) quantification of parkin, amyloid precursor protein APP and its secreted fragments (75) and CTFs in brain lysates from contra and ipsilateral hemispheres. (**G**) Detergent and FA-extracted $A\beta_{40}$ and $A\beta_{42}$ levels in contralateral and ipsilateral (parkin injected) 3xTg-AD mouse brain. (**H**) Western blot of immunoprecipitated brain lysates and (**I**) spectrograms of immunoprecipitated brain lysates identified and sequenced by MALDI-TOF mass spectroscopy. (**J**) Table showing the identity of sequenced peptides. Asterisk is significantly different to contralateral, $P < 0.05$, *t*-test. Data are mean ± SD; $n = 8$ for western blot and ELISA, $n = 3$ for MADLI-TOF.

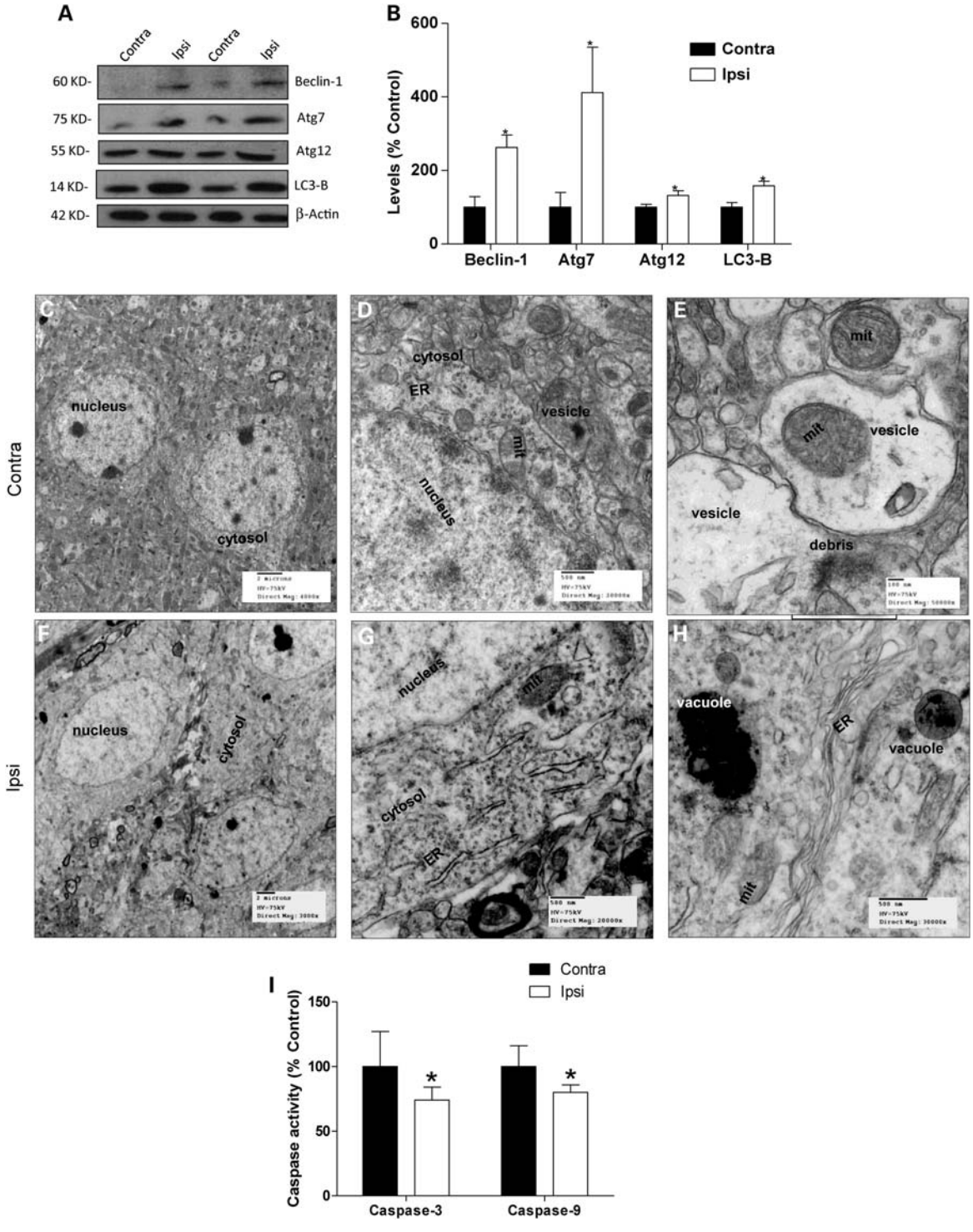


**Figure 2.** Beclin-dependent autophagic molecular steps and EM reveal parkin meditation of autophagic clearance in 3xTg-AD mice. (**A**) Western blot analysis and (**B**) quantification of autophagic pathway proteins, including beclin-1, Atg7, Atg12 and LC3-B levels in contra and ipsilateral hemispheres. Electron microscope (EM) scans of the cortex in 3xTg-AD mice showing accumulation of vesicles in the cytosol and fragmented ER (**C** and **D**) and defective mitochondria and molecular debris in vesicles (**E**). Cortical sections of parkin-injected hemispheres showing (**F**) clear cytosol and distinct nuclei, (**G**) mitochondria and healthy ER and (**H**) vacuoles packed with molecular and cellular debris in a clear and healthy looking cytosol. ER, endoplasmic reticulum; mit, mitochondria. (**I**) Histogram represents caspase-3 and 9 activities. Asterisk is significantly different to contralateral, $P < 0.05$, *t*-test. Data are mean $\pm$ SD; $n = 8$ for ELISA. $n = 3$ for EM.

perhaps due to failure of clearance mechanisms. Parkin injection into the ipsilateral hemisphere was associated with reduction in cytosolic vesicles (Fig. 2F and G). Well-defined ER and mitochondria were also observable in the absence of any vesicles in parkin-injected hemispheres (Fig. 2G and H), suggesting that parkin expression may be involved in the

clearance of vesicles. Higher magnification of parkin-injected hemispheres revealed normal ER and mitochondria and the absence of vesicular accumulation probably due to packaging of vesicles into larger vacuoles (Fig. 2H), indicating parkin-mediated clearance of vesicles containing molecular and cellular debris. These data suggest abnormal accumulation of vesicles within the cytoplasm of neurons in the 3xTg-AD mice and parkin facilitates packaging of these vesicles within digestive vacuoles and subsequent clearance of defective organelles, molecular and cellular debris.

To test whether parkin-mediated autophagic clearance affects cell survival, we measured the activities of caspase-3 and caspase-9 in detergent-extracted lysates of 3xTg-AD brain hemispheres. A significant (28%, $P < 0.05$) reduction in caspase-3 (Fig. 2I) activity was observed in parkin-injected ($P < 0.05$, $n = 8$) compared with contralateral hemispheres, indicating that lentiviral parkin expression may counteract mechanisms of cell loss. Further analysis showed a significant reduction (21%) in caspase-9 (Fig. 2I) activity in parkin-injected brains, suggesting that parkin restores mitochondrial integrity in 3xTg-AD mice.

### Histology shows parkin reduces intracellular Aβ levels and extracellular Aβ plaque

We took an independent approach to examine parkin effects on Aβ levels, using immunohistochemistry (IHC). Anti-Aβ (6E10) staining of 3xTg-AD brains showed intraneuronal Aβ accumulations in neurons of deep cortical layers (Fig. 3A insert and B) and layers of the CA1 region of the hippocampus (Fig. 3A arrows). Parkin-injected hemispheres revealed less immunoreactivity in the ipsilateral compared with the contralateral hemisphere (Fig. 3A and C, arrows). Higher magnification showed significantly (50% by stereology) more Aβ staining in the contralateral cortex (Fig. 3B) compared with parkin-injected (Fig. 3C) hemispheres ($P < 0.05$, $n = 7$). Strong 6E10 staining was also observed in the entorhinal cortex in the contralateral hemisphere (Fig. 3D) compared with parkin-injected (Fig. 3E) hemispheres. Similarly, specific anti-human $A\beta_{42}$ antibody showed a significant (35% by stereology) reduction in $A\beta_{42}$ staining in the hippocampus of parkin-injected (Fig. 3G) compared with contralateral (Fig. 3F) hemispheres. Staining of cortical sections with human anti-$A\beta_{42}$ also showed a significant decrease (41% by stereology, $P < 0.05$) of staining in parkin-injected (Fig. 3I) compared with contralateral (Fig. 3H) hemispheres. We further examined whether the levels of intracellular Aβ were correlated with extracellular plaque deposition. We performed thioflavin-S staining of serial sections of the entorhinal cortex, which is medially bordered by the parasubiculum, and laterally by the perirhinal cortex; rostrally and medially, it is bordered by the piriform cortex, whereas caudally and dorsally it is bordered by the postrhinal cortex. The entorhinal cortex showed more plaque formation in the contralateral (Fig. 3J) compared with parkin-injected (Fig. 3K) hemispheres, suggesting that parkin decreases intracellular Aβ, which may lead to reduction in extracellular Aβ deposition. These data are consistent with our results using ELISA and western blot analysis.

To examine the health of brain tissue after 3 months of parkin injection, we performed silver and glial fibrillary acidic protein (GFAP) staining to further assess cell loss in these animals. No noticeable differences in silver-positive cells were detected in the hippocampus between the ipsilateral (Fig. 3M and O) and contralateral hemispheres (Fig. 3L and N), but an increase (24% by stereology, $P < 0.05$) in silver staining was observed in the cortex of the contralateral (Fig. 3P) compared with parkin-injected (Fig. 3Q) hemispheres. No differences in GFAP staining were also observed in the hippocampus (data not shown), but a significant decrease (21% by stereology, $P < 0.05$) was observed in the cortex of parkin-injected (Fig. 3S, $n = 7$) compared with contralateral hemispheres (Fig. 3R). GFAP staining was also significantly decreased (27% by stereology, $P < 0.05$) in the entorhinal cortex of parkin-injected (Fig. 3U) compared with the contralateral (Fig. 3T) hemispheres. These data suggest that no cell loss was observed in the hippocampus but parkin reduced cell loss in the cortex of 3xTg-AD mice.

### High-frequency [$^1$H]-$^{13}$C nuclear magnetic resonance spectroscopy suggests that parkin-facilitated clearance of defective mitochondria attenuates oxidative stress and restores TCA cycle activity

To determine whether parkin expression also reduced Aβ-associated oxidative stress and mitochondrial metabolism, we performed high-frequency [$^1$H]-$^{13}$C nuclear magnetic resonance (NMR) spectroscopy to compare parkin and Lac-Z injected 3xTg-AD hemispheres. This method allowed us to measure mitochondrial TCA cycle activity and lactate production. Examination of succinate as an indicator of TCA cycle metabolism showed a significant (58%) decrease ($P < 0.05$, $n = 4$) in the flux of $^{13}$C label from [1-$^{13}$C] glucose into succinate C2/C3 in contralateral 3xTg-AD hemispheres compared with age-matched wild-type (WT) control brains (Fig. 4A). Flux of $^{13}$C into succinate C2/C3 was significantly (45%) increased in parkin-injected compared with contralateral hemispheres (Fig. 4A). Succinate (Fig. 4B) was significantly (135%) decreased in contralateral hemispheres compared with the WT, but succinate levels were significantly increased (48%) in parkin-injected (Fig. 4B) brains compared with contralateral hemispheres. These data suggest a decrease in TCA cycle activity in 3xTg-AD and parkin reversal of Aβ effects on TCA cycle function. We then traced the fate of $^{13}$C into the cytosolic compartment (Fig. 4G), particularly lactate (33). No significant difference in $^{13}$C flux into lactate C3 was observed between WT and 3xTg-AD brains (Fig. 4A). However, total lactate levels were significantly increased (47%) in 3xTg-AD brains compared with control, but lactate was decreased in parkin-injected hemispheres compared with contralateral hemispheres (Fig. 4B), suggesting a decrease in oxidative stress in the parkin-injected animals.

The decrease in mitochondrial metabolism led us to examine glutamate (31) synthesis as a by-product of TCA cycle and an important neurotransmitter (Fig. 4G). Flux of $^{13}$C into glutamate C4 was significantly (39%) decreased in 3xTg-AD hemispheres compared with the WT, but reduction was blocked in parkin-injected hemispheres (Fig. 4C). Glutamate levels were significantly (74%) decreased in 3xTg-AD

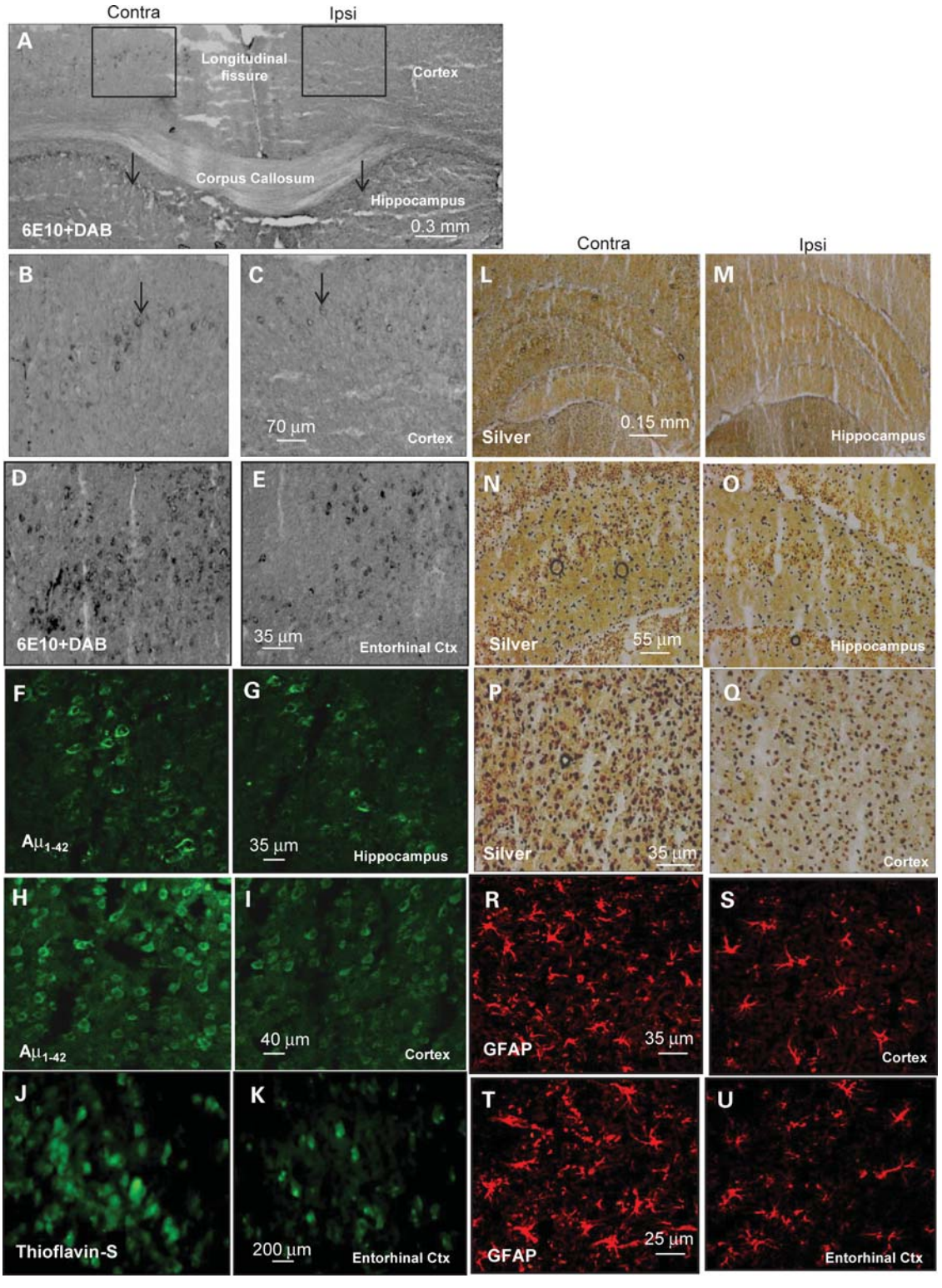


**Figure 3.** Histology shows that parkin-mediated autophagy reduces intracellular Aβ levels and extracellular Aβ plaque. (**A**) 6E10-3, 3′-diaminobenzidine (DAB) staining of 20 μm thick brain sections under ×4 magnification showing the contralateral and ipsilateral (parkin-injected) hemispheres. Arrows indicate the CA1 hippocampus region showing immunoreactivity to Aβ. (**B** and **C**) Higher magnification of inserts showing Aβ immunoreactivity (arrows) in deep cortical layers. (**D** and **E**) 6E10-DAB staining of entorhinal cortex and (**F** and **G**) human-specific $A\beta_{42}$ immunostainning of hippocampus brain sections. (**H** and **I**) Human-specific $A\beta_{42}$ immunostainning of the cortex. (**J** and **K**) Brain sections show thioflavin-s-positive staining of the entorhinal cortex. (**L** and **M**) Silver staining of hippocampus at ×4, and (**N** and (**O** higher magnification (×20) view of hippocampal slices. (**P** and **Q**) Silver staining of sections of deep cortical layers. Sections stained with GFAP in the (**R** and **S**) cortex and (**T** and **U**) the entorhinal cortex.

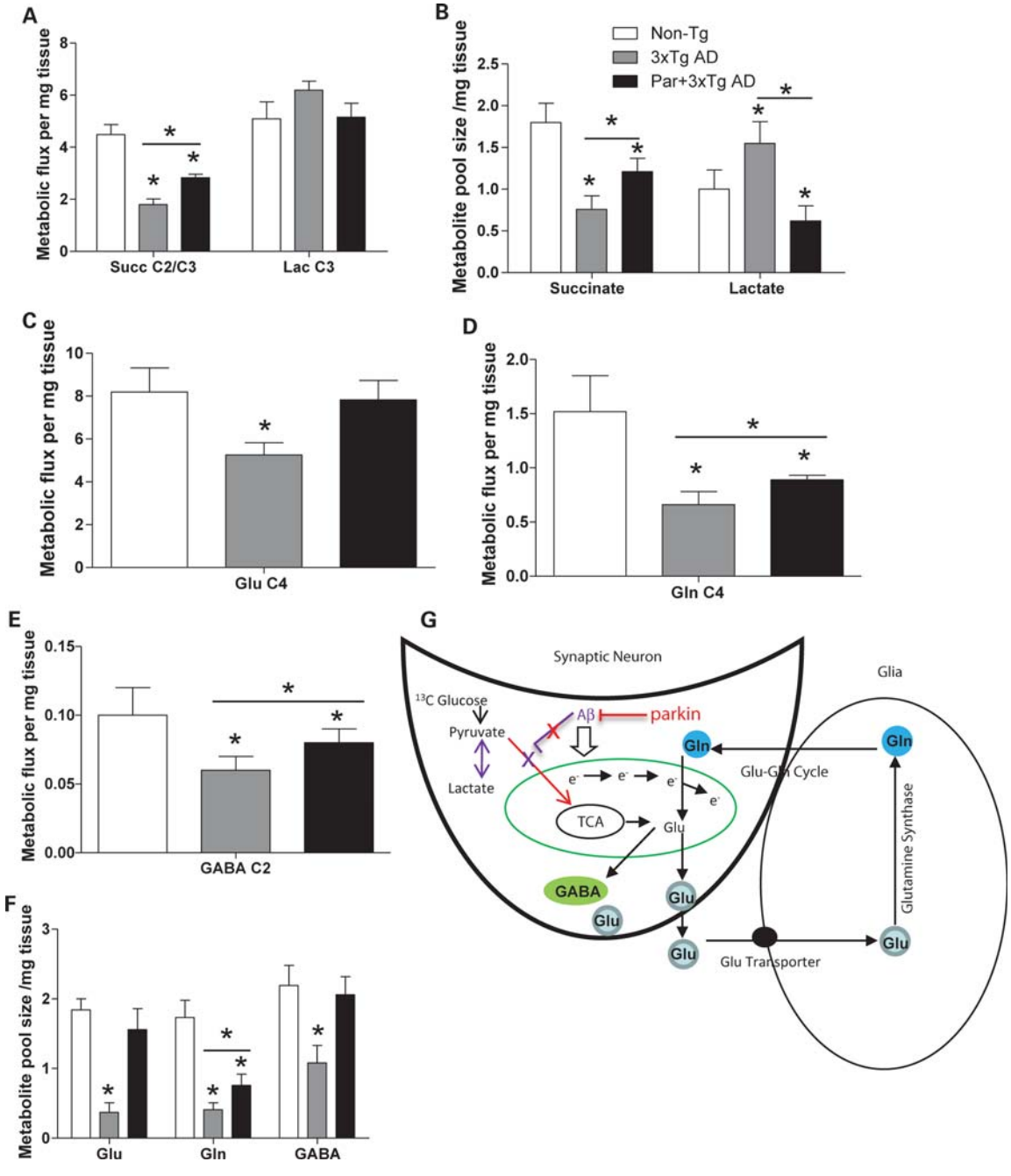


**Figure 4.** High-frequency [$^{1}$H]-$^{13}$C NMR spectroscopy suggests that parkin-facilitated clearance of defective mitochondria attenuates oxidative stress and restores TCA cycle activity. High-frequency [$^{1}$H]-$^{13}$C NMR spectroscopy showing (**A**) histograms that represent metabolic flux of $^{13}$C label from glucose into Succ C2/C3 and Lac C3; (**B**) metabolic pool size of Succ and Lac; (**C**) metabolic flux into Glu C4, (**D**) Gln C4 and (**E**) GABA C2; (**F**) metabolic pool size of Glu, Gln and GABA. (**G**) Schematic representation of neuronal and astrocytic compartments, depicting Glu–Gln cycle, cytosolic and mitochondrial metabolism and the effects of Aβ on cell compartmentalization. Aβ decreases $^{13}$C flux into the mitochondria and stimulates Lac production resulting in oxidative stress. Aβ decreases TCA-derived neurotransmitters Glu and GABA and depresses the Glu–Gln cycle. Parkin decreases the levels of intracellular Aβ, enhances $^{13}$C flux into mitochondrial TCA cycle and decreases Lac production, thus alleviating oxidative stress. Parkin reverses Aβ-induced decrease in Glu and GABA levels via amelioration of TCA cycle activity, which is independent of Glu–Gln cycle, restoring synaptic neurotransmitter balance. TCA, tricarboxylic acid; Glu, glutamate; Gln, glutamine; GABA, γ-amino butyric acid; Succ, succinate; Lac, lactate. Asterisk is significantly different to contralateral or as indicated, $P < 0.05$, *t*-test. Data are mean ± SD; $n = 4$.

brains compared with the WT (Fig. 4F), but this reduction was reversed back to control levels in parkin-injected brains. We tested whether glutamate synthesis was affected by recycling via the glutamate–glutamine (Glu–Gln) cycle (Fig. 4G). Flux of $^{13}$C into glutamine C4 was significantly (60%) decreased in 3xTg-AD compared with the WT and parkin-injected 3xTg-AD hemispheres (Fig. 4D). Glutamine was significantly (76%) decreased in 3xTg-AD hemispheres compared with WT brains (Fig. 4F). Glutamine was significantly (40%) reversed in parkin-injected compared with non-

injected 3xTg-AD brains. These data suggest that restoration of glutamate levels in parkin-injected 3xTg-AD brains is affected by TCA-derived glutamate and not by recycling via the neuronal–glial Glu–Gln cycle (Fig. 4G).

We then examined whether alteration in glutamate synthesis affected the levels of the neurotransmitter GABA, which depends on glutamate as a precursor. Flux of $^{13}C$ into GABA C2 was significantly (40%) decreased in 3xTg-AD hemispheres compared with the WT, but this reduction in flux was significantly reversed (24%) in parkin-injected hemispheres (Fig. 4E). GABA levels were significantly (51%) decreased in 3xTg-AD hemispheres compared with WT brains (Fig. 4F), but GABA levels were significantly (94%) reversed in parkin-injected hemispheres. These data suggest that parkin prevents a reduction in glutamate synthesis in 3xTg-AD brains, while subsequently restores normal levels of GABA.

## DISCUSSION

We previously showed that parkin ubiquitinated and cleared intraneuronal $A\beta_{42}$ in lentiviral gene transfer models (31,32,34). In this work, we tested whether parkin could facilitate autophagic clearance, reduce intracellular Aβ and extracellular plaque and reverse Aβ-induced defects in 3xTg-AD mice. Lentiviral gene delivery of parkin showed protein expression up to 3 months post-injection. We showed that parkin ubiquitinates intracellular Aβ *in vivo*, stimulates the beclin molecular cascade of autophagy and clears vesicles-containing debris and defective mitochondria in 3xTg-AD mice. Intracellular Aβ accumulation is pathological and directly inhibits the Ub-proteasome system leading to protein accumulation (32,35,36) in animal models and cell culture (35,37). In 3xTg-AD mice, proteasome inhibition is concurrent with oligomeric Aβ accumulation within neuronal cell bodies (38,39), which results in higher Aβ levels. The reduction in proteasomal activity and accumulation of Aβ may result in organelle damage, including the ER and mitochondria. Blockage of the proteasome and aggregation of toxic proteins induce autophagy (40,41) concurrent with ubiquitination (42,43). We observed reduction in TCA cycle activity and increase in molecular markers of autophagy and defective mitochondria, suggesting depletion of cellular energy that would induce autophagy and result in autophagosome accumulation. Accumulation of vesicles loaded with debris and defective organelles within the cytosol suggests impairment of clearance mechanisms. Our studies suggest that parkin facilitates clearance of vesicles, fragmented ER and defective mitochondria, contributing to disposal of damaged organelles and cellular and molecular debris, perhaps via synergistic effects between ubiquitination and autophagy.

An increase in beclin levels is correlated with autophagic activity (44,45), and a decrease in beclin is associated with aging and neurodegenerative diseases (46). Parkin expression increased beclin levels, suggesting activation of beclin-dependent autophagy to facilitate the clearance of cytosolic vesicles. Deletion of autophagic components, including Atg7, suppresses macroautophagy (47,48), while LC3 links ubiquitinated protein aggregates to the autophagosome for degradation (49,50). We also observed an increase in Atg7, Atg12 and LC3-B levels in the presence of parkin, indicating activation of the beclin-autophagic cascade. Taken together, these data suggest that Aβ accumulation may induce beclin-independent autophagy, perhaps via mamalian target of rapamaycin-dependent pathways resulting in accumulation of vesicles, and parkin ubiquitinates Aβ and activates beclin-dependent mechanisms to facilitate clearance. Our results are consistent with previous observations that undegraded autophagosomes are present in human advanced stages (51) and animal models (52) of AD, suggesting that the lack of autophagosome–lysosome fusion can lead to leaky vacuoles and pathogenic accumulation of Aβ (53).

Parkin-mediated clearance of intracellular Aβ and decreased plaque deposition are consistent with findings that intracellular Aβ accumulation precedes extracellular plaques in transgenic animals (6,54–60), and suggest that accumulation of intraneuronal Aβ is an early event in AD pathology. Intraneuronal Aβ levels decrease in 3xTg-AD mice and Down syndrome brains as extracellular plaques accumulate (9–11). Reduction in Aβ levels results in the elimination of brain atrophy, which is associated with mild cognitive impairment, in which intraneuronal Aβ accumulates in regions that are prone to the development of early AD pathology, such as the hippocampus and the entorhinal cortex (61). The decrease in cell death associated with the reduction in Aβ levels is consistent with evidence that lysis of neurons with intracellular Aβ leads to Aβ dispersion in the extracellular space (62,63). In the 3xTg-AD model, clearance of intraneuronal Aβ was shown to follow removal of extracellular Aβ plaques (64), but when the pathology re-emerges, extracellular plaques follow the accumulation of intraneuronal Aβ (9). These observations indicate a balance between extracellular and intracellular Aβ that can be therapeutically exploited to reduce amyloid burden in AD.

In another APP transgenic model (Tg2576), Aβ is observed in mitochondria (65). Accumulation of intracellular Aβ in mitochondria is associated with diminished enzymatic activity of respiratory chain complexes III and IV, and reduced rate of oxygen consumption (66). Decreased glucose metabolism is also observed in the brains of AD patients (67), perhaps leading to adenosine triphosphate (ATP) depletion and autophagic alterations. We observe defective mitochondria in 3xTg-AD mice and parkin clears vesicle-containing mitochondria. These observations led us to investigate the effects of parkin on Aβ-associated mitochondrial defects described in human patients and animal models of AD (68). Accumulation of Aβ decreases TCA cycle activity (Fig. 4G) and increases lactate production, suggesting an increased level of oxidative stress. Parkin reverses Aβ-induced inhibition of mitochondrial TCA cycle and attenuates cytosolic lactate production, suggesting that the clearance of intraneuronal Aβ reduces oxidative stress (27–30), and may modulate autophagy. Parkin-associated increase in mitochondrial activity leads to increased aerobic respiration, consistent with parkin role as a modulator of mitochondrial function (17–25).

Intraneuronal Aβ is involved in synaptic dysfunction, which could underlie cognitive deficits in AD and transgenic animal models. Indeed, the 3xTg-AD mice develop intraneuronal Aβ

accumulation when cognitive deficits are first detected (68). Removal of intraneuronal Aβ with immunotherapy restores cognitive function (68), but intraneuronal Aβ results in profound deficits in long-term potentiation (LTP) (59), which underlies memory (69). Furthermore, increased Ub C-terminal hydrolase L1 levels rescues Aβ-induced LTP deficits (70), further suggesting a possible involvement of the Ub-proteasome system in the maintenance of synaptic function. Magnetic resonance spectroscopy (MRS) demonstrates a significant decrease in glutamate levels in 3xTg-AD mice, consistent with previous data from other APP transgenic mouse models (7,71,72). Parkin increased glutamate back to control levels, indicating restoration of neurotransmitter synthesis. Parkin did not affect glutamine levels, suggesting that the increase in glutamate synthesis was independent of the Glu–Gln cycle. We further tested the effects of parkin on the inhibitory neurotransmitter GABA. Aβ-induced decrease in glutamate was simultaneous with the decrease in GABA levels, and parkin reversed GABA levels (Fig. 4G), suggesting that Aβ suppresses excitatory glutamate and induces dysfunction in inhibitory transmission, leading to modification in neurotransmitter equilibrium and destabilization of neuronal circuit activity (73). Furthermore, our studies are consistent with previous data suggesting that $^{13}C$ flux through succinate is a good indicator of TCA cycle activity in relation to the GABA shunt, because GABAergic neurons account for less than one-third of the overall cerebral TCA cycle activity, which depends on GABA/glutamate pool size ratio in the mouse brain (74). These studies should be further investigated to provide more evidence that intracellular Aβ has detrimental roles on neurotransmitter levels, independent of cell death. Parkin-mediated autophagic clearance could be an alternative strategy to clear brain Aβ and restore neurotransmitter equilibrium and synaptic dysfunction.

The E3-Ub ligase parkin stimulates autophagic clearance and reduces toxic intracellular Aβ levels and neurodegenerative death. Clearance of intraneuronal Aβ results in a decrease in extracellular plaque buildup, suggesting that intraneuronal Aβ precedes plaque formation. Parkin-mediated clearance of Aβ prevents oxidative stress and mitochondrial dysfunction and may restore ATP production to modulate autophagy. Increased TCA cycle activity restores loss of mitochondrial contribution to glutamate synthesis and reverses the decrease in GABA levels, suggesting return of neurotransmitter equilibrium that underlies neuronal networks. Thus, parkin is a candidate gene therapy to promote autophagic clearance, degrade intraneuronal Aβ, limit extracellular plaque deposition and prevent AD-associated pathology.

## MATERIALS AND METHODS

### Stereotaxic injection

Stereotaxic surgery was performed to inject lentiviral parkin into the right, and LacZ into the left CA1 region of the hippocampus of 1–1.5-year-old 3xTg-AD mice using Paxinos and Watson mouse atlas for coordinates, including 1.7 mm lateral, 2.2 mm ventral and 2 mm posterior. Viral stocks (6 μl) were injected as described in ref. (31) at a rate of 0.2 μl/min. Animals were injected into the left hippocampus with a lentiviral–LacZ vector at $1 \times 10^{10}$ mutliplicity of infection (m.o.i.), and the right hippocampus with $1 \times 10^{10}$ m.o.i. lentiviral parkin. A total of 23 mice were injected and sacrificed 3 months post-injection.

### Western blot analysis

Brain tissues were homogenized in 1x STEN buffer [50 mM Tris (pH 7.6), 150 mM NaCl, 2 mM thylenediaminetetraacetic acid, 0.2% nonyl phenoxypolyethoxylethanol-40, 0.2% bovine serum albumin, 20 mM phenylmethanesulfonylfluoride and protease cocktail inhibitor], centrifuged at 10 000*g* for 20 min at 4°C and the supernatant containing the soluble fraction of proteins was collected. The supernatant was analyzed by western blot on sodium dodecyl sulfate NuPAGE 4–12% Bis–Tris gel (Invitrogen, Inc.). Protein estimation was performed using BioRad protein assay (BioRad Laboratories Inc., Hercules, CA, USA). Parkin and Aβ were immunoprobed as indicated (31). Full-length APP and CTFs were probed with C1.61 (1:1000) antibody (Paul Mathews, Nathan Kline Institute), secreted APPα was probed with 2B3 (1:1000) antibody (IBL International) and APPβ with 22C11 (1:1000) antibody (Millipore). Autophagy antibodies, including beclin (1:1000), Atg7 (1:1000), Atg12 (1:1000) and LC3-B (1:1000), were used to probe according to autophagy antibody sampler kit 4445 (Cell Signaling, Inc.). Immunoprecipitation was performed using (PD4) anti-Ub (1:100) antibody (Chemicon International) or (6E10) anti-APP (1:100) antibody (Signet, Dedham, MA, USA). Western blots were quantified by densitometry using Quantity One 4.6.3 software (Bio Rad). Densitometry was obtained as arbitrary numbers measuring band intensity and all values were converted to % control. Eight animals were used to compare contra and ipsilateral hemispheres, and the data were analyzed as mean ± SD and statistical comparison of variables was obtained by *t*-test, $P < 0.05$.

### Histology

To perform immunohistochemical analysis of brain tissues, animals were deeply anesthetized with a mixture of xylazine and ketamine (1:8), washed with 1X saline for 1 min and then perfused with 4% paraformaldehyde (PFA) for 15–20 min. Brains were quickly dissected out and immediately stored in 4% PFA for 24 h at 4°C, and then transferred to 30% sucrose at 4°C for 48 h. After perfusion and sucrose cryoprotection, tissues were cut using a cryostat into 20 μm thick sections and stored at −20°C. IHC was performed on 20 μm thick brain sections and compared between contra and ipsilateral hemispheres. $A\beta_{42}$ was probed (1:200) with rabbit polyclonal-specific anti-$A\beta_{42}$ antibody (Zymed) or 6E10 followed by 3, 3′-diaminobenzidine staining. Further staining was performed to assess neural disintegrative degeneration in animal models using FD NeuroSilver™ staining kit II (FD NeuroTechnologies, Inc., Baltimore, MD, USA), which provides high contrast and rapid silver staining for the microscopic detection of neuronal and fiber degeneration *in vivo*. Thioflavin-s staining was performed according to the manufacturer's instructions (Sigma). Total cell counts in cortical subfields were obtained by a blinded investigator using

unbiased stereology analysis (Stereologer, Systems Planning and Analysis, Chester, MD, USA). A minimum of seven 20 μm sections were analyzed from 400 μm in each direction from the injection site in the ispilateral area, and an equivalent size area within the same region in the contralateral area. The multi-level sampling design in the Stereologer software, based on the optical fractionator sampling method, was used to estimate positive cell numbers. Seven mice were used for IHC.

### Caspase-3 and caspase-9 fluorometric activity assay

To measure caspase-3 activity in the animal models, we used EnzChek® caspase-3 assay kit #1 (Invitrogen, Molecular Probes, Inc.) on total hemisphere extracts and Z-DEVD-AMC substrate and read the absorbance according to the manufacturer's protocol. We also used AC-LEHD-AMC substrate (Invitrogen, Molecular Probes, Inc.) to measure caspase-9 activity according to the manufacturer's protocol.

### Aβ ELISA

Human specific $A\beta_{40}$ and $A\beta_{42}$ ELISA (Biosource, Inc.) were performed using 50 μl (1 μg/μl) of whole hemisphere brain lysates, detected with 50 μl human $A\beta_{40}$ or $A\beta_{42}$ primary antibody (3 h) and 100 μl anti-rabbit antibody (30 min) at RT. Extracts were incubated with stabilized chromogen for 30 min at RT and solution was stopped and read at 450 nm, according to the manufacturer's protocol.

### MALDI-TOF mass spectrometry

Immunoprecipitation was followed by western blot fractionation and SilverQuest staining (Invitrogen) of gels, and the protein bands of interest were manually excised. Protein identification was carried out on a 4800 MALDI-TOF–TOF Analyzer (Applied Biosystems, CA, USA) in reflector-positive mode and then validated in MS/MS mode as described in reference (31). Detected peptide and fragment masses were compared with the theoretical masses stored in SWISS-PROT databases using MASCOT.

### High-frequency [$^1$H]-$^{13}$C MRS

Animals were fasted overnight with free access to tap water and were intraperitoneally (i.p.) injected with [1-$^{13}$C] glucose solution (0.5 mol/l) over 10 s (0.3 ml/25–30 g body weight; 200 mg/kg). We empirically determined that 45 min was optimal for $^{13}$C labeling of metabolites in the mouse brain. So, 45 min post-injection with [1-$^{13}$C] glucose, animals were sacrificed by cervical dislocation and brains immediately homogenized in 6% ice-cold perchloric acid, 50 mM $NaH_2PO_4$. After homogenization and lyophilization, extracts were re-suspended in 0.65 ml $D_2O$ containing 2 mM sodium [$^{13}$C]formate as internal intensity and chemical shift reference (δ 171.8). Metabolite pool size was identified on $^1$H [$^{13}$C-decoupled] NMR spectra. Peak areas were adjusted for nuclear Overhauser effect, saturation and natural abundance effects and quantified by reference to [$^{13}$C] formate. Metabolite pool sizes were determined by integration of resonances in fully relaxed 400 MHz [$^{13}$C-decoupled] $^1$H spectra using N-acetylaspartate as internal intensity reference. Incorporation of $^{13}$C into isotopomers was measured in reference to [$^{13}$C] formate. All data were collected on a 9.7 Tesla Varian Spectrometer with dual $^{13}$C/$^1$H probe. [$^{13}$C-decoupled]-$^1$H spectra were acquired with 3000 scans, pulse width 45°, relaxation delay 1 s, line broadening 0.5 Hz, acquired data points 13.132 and transformation size 32 K at room temperature. [$^1$H-decoupled]-$^{13}$C spectra were acquired with 30 000 scans and 31 875 data points. Spectra were integrated and quantified using MestReNova (Master Lab Research).

### Scanning EM

Brain tissues were fixed in (1:4, v:v) 4% PFA-picric acid solution and 25% glutaraldehyde overnight, then washed 3× in 0.1 M cacodylate buffer and osmicated in 1% osmium tetroxide/1.5% potassium ferrocyanide for 3 h, followed by another 3× wash in distilled water. Samples were treated with 1% uranyl acetate in maleate buffer for 1 h, washed 3× in maleate buffer (pH 5.2), then exposed to a graded cold ethanol series up to 100% and ending with a propylene oxide treatment. Samples are embedded in pure plastic and incubated at 60°C for 1–2 days. Blocks are sectioned on a Leica ultracut microtome at 95 nm, picked up onto 100 nm formvar-coated copper grids and analyzed using a Philips Technai Spirit transmission EM.

## ACKNOWLEDGMENTS

The authors would like to acknowledge Dr R. Scott Turner (R01 AG026478) for the 3xTg-AD mice. No conflicts or commercial affiliation are associated with this manuscript.

*Conflict of Interest statement*. None declared.

## FUNDING

This work was supported by NIH NIA-KO1 AG30378 award to C.E.-H.M.

## REFERENCES

1. Glenner, G.G. and Wong, C.W. (1984) Alzheimer's disease: initial report of the purification and characterization of a novel cerebrovascular amyloid protein. *Biochem. Biophys. Res. Commun.*, **120**, 885–890.
2. Masters, C.L., Simms, G., Weinman, N.A., Multhaup, G., McDonald, B.L. and Beyreuther, K. (1985) Amyloid plaque core protein in Alzheimer disease and Down syndrome. *Proc. Natl Acad. Sci. USA*, **82**, 4245–4249.
3. Jarrett, J.T., Berger, E.P. and Lansbury, P.T. Jr. (1993) The carboxy terminus of the beta amyloid protein is critical for the seeding of amyloid formation: implications for the pathogenesis of Alzheimer's disease. *Biochemistry*, **32**, 4693–4697.
4. Younkin, S.G. (1998) The role of A beta 42 in Alzheimer's disease. *J. Physiol. Paris*, **92**, 289–292.
5. Allinson, T.M., Parkin, E.T., Turner, A.J. and Hooper, N.M. (2003) ADAMs family members as amyloid precursor protein alpha-secretases. *J. Neurosci. Res.*, **74**, 342–352.
6. Li, Q.X., Maynard, C., Cappai, R., McLean, C.A., Cherny, R.A., Lynch, T., Culvenor, J.G., Trevaskis, J., Tanner, J.E., Bailey, K.A. *et al.* (1999) Intracellular accumulation of detergent-soluble amyloidogenic A beta fragment of Alzheimer's disease precursor protein in the hippocampus of aged transgenic mice. *J. Neurochem.*, **72**, 2479–2487.

7. von Kienlin, M., Kunnecke, B., Metzger, F., Steiner, G., Richards, J.G., Ozmen, L., Jacobsen, H. and Loetscher, H. (2005) Altered metabolic profile in the frontal cortex of PS2APP transgenic mice, monitored throughout their life span. *Neurobiol. Dis.*, **18**, 32–39.
8. Takahashi, R.H., Milner, T.A., Li, F., Nam, E.E., Edgar, M.A., Yamaguchi, H., Beal, M.F., Xu, H., Greengard, P. and Gouras, G.K. (2002) Intraneuronal Alzheimer abeta42 accumulates in multivesicular bodies and is associated with synaptic pathology. *Am. J. Pathol.*, **161**, 1869–1879.
9. Oddo, S., Caccamo, A., Smith, I.F., Green, K.N. and LaFerla, F.M. (2006) A dynamic relationship between intracellular and extracellular pools of Abeta. *Am. J. Pathol.*, **168**, 184–194.
10. Gyure, K.A., Durham, R., Stewart, W.F., Smialek, J.E. and Troncoso, J.C. (2001) Intraneuronal abeta-amyloid precedes development of amyloid plaques in Down syndrome. *Arch. Pathol. Lab. Med.*, **125**, 489–492.
11. Mori, C., Spooner, E.T., Wisniewsk, K.E., Wisniewski, T.M., Yamaguch, H., Saido, T.C., Tolan, D.R., Selkoe, D.J. and Lemere, C.A. (2002) Intraneuronal Abeta42 accumulation in Down syndrome brain. *Amyloid*, **9**, 88–102.
12. Ohyagi, Y., Tsuruta, Y., Motomura, K., Miyoshi, K., Kikuchi, H., Iwaki, T., Taniwaki, T. and Kira, J. (2007) Intraneuronal amyloid beta42 enhanced by heating but counteracted by formic acid. *J. Neurosci. Methods*, **159**, 134–138.
13. Kitada, T., Asakawa, S., Hattori, N., Matsumine, H., Yamamura, Y., Minoshima, S., Yokochi, M., Mizuno, Y. and Shimizu, N. (1998) Mutations in the parkin gene cause autosomal recessive juvenile parkinsonism. *Nature*, **392**, 605–608.
14. Huang, Y., Song, Y.J., Murphy, K., Holton, J.L., Lashley, T., Revesz, T., Gai, W.P. and Halliday, G.M. (2008) LRRK2 and parkin immunoreactivity in multiple system atrophy inclusions. *Acta Neuropathol.*, **116**, 639–646.
15. Song, Y.J., Halliday, G.M., Holton, J.L., Lashley, T., O'Sullivan, S.S., McCann, H., Lees, A.J., Ozawa, T., Williams, D.R., Lockhart, P.J. *et al.* (2009) Degeneration in different parkinsonian syndromes relates to astrocyte type and astrocyte protein expression. *J. Neuropathol. Exp. Neurol.*, **68**, 1073–1083.
16. Solano, R.M., Casarejos, M.J., Menendez-Cuervo, J., Rodriguez-Navarro, J.A., Garcia de Yebenes, J. and Mena, M.A. (2008) Glial dysfunction in parkin null mice: effects of aging. *J. Neurosci.*, **28**, 598–611.
17. Geisler, S., Holmstrom, K.M., Skujat, D., Fiesel, F.C., Rothfuss, O.C., Kahle, P.J. and Springer, W. (2010) PINK1/Parkin-mediated mitophagy is dependent on VDAC1 and p62/SQSTM1. *Nat. Cell Biol.*, **12**, 119–131.
18. Narendra, D., Tanaka, A., Suen, D.F. and Youle, R.J. (2008) Parkin is recruited selectively to impaired mitochondria and promotes their autophagy. *J. Cell Biol.*, **183**, 795–803.
19. Park, J., Kim, Y. and Chung, J. (2009) Mitochondrial dysfunction and Parkinson's disease genes: insights from Drosophila. *Dis. Model. Mech.*, **2**, 336–340.
20. Vives-Bauza, C., Zhou, C., Huang, Y., Cui, M., de Vries, R.L., Kim, J., May, J., Tocilescu, M.A., Liu, W., Ko, H.S. *et al.* (2010) PINK1-dependent recruitment of Parkin to mitochondria in mitophagy. *Proc. Natl Acad. Sci. USA*, **107**, 378–383.
21. Kanki, T., Wang, K., Cao, Y., Baba, M. and Klionsky, D.J. (2009) Atg32 is a mitochondrial protein that confers selectivity during mitophagy. *Dev. Cell*, **17**, 98–109.
22. Kirkin, V., McEwan, D.G., Novak, I. and Dikic, I. (2009) A role for ubiquitin in selective autophagy. *Mol. Cell*, **34**, 259–269.
23. Novak, I., Kirkin, V., McEwan, D.G., Zhang, J., Wild, P., Rozenknop, A., Rogov, V., Lohr, F., Popovic, D., Occhipinti, A. *et al.* (2010) Nix is a selective autophagy receptor for mitochondrial clearance. *EMBO Rep.*, **11**, 45–51.
24. Okamoto, K., Kondo-Okamoto, N. and Ohsumi, Y. (2009) Mitochondria-anchored receptor Atg32 mediates degradation of mitochondria via selective autophagy. *Dev. Cell*, **17**, 87–97.
25. Wild, P. and Dikic, I. (2010) Mitochondria get a Parkin' ticket. *Nat. Cell Biol.*, **12**, 104–106.
26. Sutovsky, P., Moreno, R.D., Ramalho-Santos, J., Dominko, T., Simerly, C. and Schatten, G. (1999) Ubiquitin tag for sperm mitochondria. *Nature*, **402**, 371–372.
27. Markesbery, W.R. (1997) Oxidative stress hypothesis in Alzheimer's disease. *Free Radic. Biol. Med.*, **23**, 134–147.
28. McGeer, P.L., Rogers, J. and McGeer, E.G. (2006) Inflammation, anti-inflammatory agents and Alzheimer disease: the last 12 years. *J. Alzheimers Dis.*, **9**, 271–276.
29. Rozemuller, J.M., Eikelenboom, P. and Stam, F.C. (1986) Role of microglia in plaque formation in senile dementia of the Alzheimer type. An immunohistochemical study. *Virchows Arch. B Cell Pathol. Incl. Mol. Pathol.*, **51**, 247–254.
30. Wyss-Coray, T. (2006) Inflammation in Alzheimer disease: driving force, bystander or beneficial response? *Nat. Med.*, **12**, 1005–1015.
31. Burns, M.P., Zhang, L., Rebeck, G.W., Querfurth, H.W. and Moussa, C.E. (2009) Parkin promotes intracellular Abeta1-42 clearance. *Hum. Mol. Genet.*, **18**, 3206–3216.
32. Rosen, K.M., Moussa, C.E., Lee, H.K., Kumar, P., Kitada, T., Qin, G., Fu, Q. and Querfurth, H.W. (2010) Parkin reverses intracellular beta-amyloid accumulation and its negative effects on proteasome function. *J. Neurosci. Res.*, **88**, 167–178.
33. de Garavilla, L., Vergnolle, N., Young, S.H., Ennes, H., Steinhoff, M., Ossovskaya, V.S., D'Andrea, M.R., Mayer, E.A., Wallace, J.L., Hollenberg, M.D. *et al.* (2001) Agonists of proteinase-activated receptor 1 induce plasma extravasation by a neurogenic mechanism. *Br. J. Pharmacol.*, **133**, 975–987.
34. Rebeck, G.W., Hoe, H.S. and Moussa, C.E. (2010) [beta]-Amyloid1-42 gene transfer model exhibits intraneuronal amyloid, gliosis, tau phosphorylation, and neuronal loss. *J. Biol. Chem.*, **285**, 7440–7446.
35. Almeida, C.G., Takahashi, R.H. and Gouras, G.K. (2006) Beta-amyloid accumulation impairs multivesicular body sorting by inhibiting the ubiquitin-proteasome system. *J. Neurosci.*, **26**, 4277–4288.
36. Gregori, L., Fuchs, C., Figueiredo-Pereira, M.E., Van Nostrand, W.E. and Goldgaber, D. (1995) Amyloid beta-protein inhibits ubiquitin-dependent protein degradation in vitro. *J. Biol. Chem.*, **270**, 19702–19708.
37. Oh, S., Hong, H.S., Hwang, E., Sim, H.J., Lee, W., Shin, S.J. and Mook-Jung, I. (2005) Amyloid peptide attenuates the proteasome activity in neuronal cells. *Mech. Ageing Dev.*, **126**, 1292–1299.
38. Oddo, S., Caccamo, A., Tran, L., Lambert, M.P., Glabe, C.G., Klein, W.L. and LaFerla, F.M. (2006) Temporal profile of amyloid-beta (Abeta) oligomerization in an in vivo model of Alzheimer disease. A link between Abeta and tau pathology. *J. Biol. Chem.*, **281**, 1599–1604.
39. Tseng, B.P., Green, K.N., Chan, J.L., Blurton-Jones, M. and LaFerla, F.M. (2008) Abeta inhibits the proteasome and enhances amyloid and tau accumulation. *Neurobiol. Aging*, **29**, 1607–1618.
40. Iwata, A., Christianson, J.C., Bucci, M., Ellerby, L.M., Nukina, N., Forno, L.S. and Kopito, R.R. (2005) Increased susceptibility of cytoplasmic over nuclear polyglutamine aggregates to autophagic degradation. *Proc. Natl Acad. Sci. USA*, **102**, 13135–13140.
41. Ravikumar, B., Vacher, C., Berger, Z., Davies, J.E., Luo, S., Oroz, L.G., Scaravilli, F., Easton, D.F., Duden, R., O'Kane, C.J. *et al.* (2004) Inhibition of mTOR induces autophagy and reduces toxicity of polyglutamine expansions in fly and mouse models of Huntington disease. *Nat. Genet.*, **36**, 585–595.
42. Nedelsky, N.B., Todd, P.K. and Taylor, J.P. (2008) Autophagy and the ubiquitin-proteasome system: collaborators in neuroprotection. *Biochim. Biophys. Acta*, **1782**, 691–699.
43. Wong, E. and Cuervo, A.M. (2010) Autophagy gone awry in neurodegenerative diseases. *Nat. Neurosci.*, **13**, 805–811.
44. Erlich, S., Shohami, E. and Pinkas-Kramarski, R. (2006) Neurodegeneration induces upregulation of Beclin 1. *Autophagy*, **2**, 49–51.
45. Pickford, F., Masliah, E., Britschgi, M., Lucin, K., Narasimhan, R., Jaeger, P.A., Small, S., Spencer, B., Rockenstein, E., Levine, B. *et al.* (2008) The autophagy-related protein beclin 1 shows reduced expression in early Alzheimer disease and regulates amyloid beta accumulation in mice. *J. Clin. Invest.*, **118**, 2190–2199.
46. Shibata, M., Lu, T., Furuya, T., Degterev, A., Mizushima, N., Yoshimori, T., MacDonald, M., Yankner, B. and Yuan, J. (2006) Regulation of intracellular accumulation of mutant Huntingtin by Beclin 1. *J. Biol. Chem.*, **281**, 14474–14485.
47. Hara, T., Nakamura, K., Matsui, M., Yamamoto, A., Nakahara, Y., Suzuki-Migishima, R., Yokoyama, M., Mishima, K., Saito, I., Okano, H. *et al.* (2006) Suppression of basal autophagy in neural cells causes neurodegenerative disease in mice. *Nature*, **441**, 885–889.
48. Komatsu, M., Waguri, S., Chiba, T., Murata, S., Iwata, J., Tanida, I., Ueno, T., Koike, M., Uchiyama, Y., Kominami, E. *et al.* (2006) Loss of

autophagy in the central nervous system causes neurodegeneration in mice. *Nature*, **441**, 880–884.
49. Bjorkoy, G., Lamark, T., Brech, A., Outzen, H., Perander, M., Overvatn, A., Stenmark, H. and Johansen, T. (2005) p62/SQSTM1 forms protein aggregates degraded by autophagy and has a protective effect on huntingtin-induced cell death. *J. Cell Biol.*, **171**, 603–614.
50. Tan, J.M., Wong, E.S., Dawson, V.L., Dawson, T.M. and Lim, K.L. (2007) Lysine 63-linked polyubiquitin potentially partners with p62 to promote the clearance of protein inclusions by autophagy. *Autophagy*, **4**.
51. Lee, J.H., Yu, W.H., Kumar, A., Lee, S., Mohan, P.S., Peterhoff, C.M., Wolfe, D.M., Martinez-Vicente, M., Massey, A.C., Sovak, G. *et al.* (2010) Lysosomal proteolysis and autophagy require presenilin 1 and are disrupted by Alzheimer-related PS1 mutations. *Cell*, **141**, 1146–1158.
52. Yu, W.H., Cuervo, A.M., Kumar, A., Peterhoff, C.M., Schmidt, S.D., Lee, J.H., Mohan, P.S., Mercken, M., Farmery, M.R., Tjernberg, L.O. *et al.* (2005) Macroautophagy—a novel beta-amyloid peptide-generating pathway activated in Alzheimer's disease. *J. Cell Biol.*, **171**, 87–98.
53. Kaasik, A., Rikk, T., Piirsoo, A., Zharkovsky, T. and Zharkovsky, A. (2005) Up-regulation of lysosomal cathepsin L and autophagy during neuronal death induced by reduced serum and potassium. *Eur. J. Neurosci.*, **22**, 1023–1031.
54. Chui, D.H., Tanahashi, H., Ozawa, K., Ikeda, S., Checler, F., Ueda, O., Suzuki, H., Araki, W., Inoue, H., Shirotani, K. *et al.* (1999) Transgenic mice with Alzheimer presenilin 1 mutations show accelerated neurodegeneration without amyloid plaque formation. *Nat. Med.*, **5**, 560–564.
55. Knobloch, M., Konietzko, U., Krebs, D.C. and Nitsch, R.M. (2007) Intracellular Abeta and cognitive deficits precede beta-amyloid deposition in transgenic arcAbeta mice. *Neurobiol. Aging*, **28**, 1297–1306.
56. Kuo, Y.M., Beach, T.G., Sue, L.I., Scott, S., Layne, K.J., Kokjohn, T.A., Kalback, W.M., Luehrs, D.C., Vishnivetskaya, T.A., Abramowski, D. *et al.* (2001) The evolution of A beta peptide burden in the APP23 transgenic mice: implications for A beta deposition in Alzheimer disease. *Mol. Med.*, **7**, 609–618.
57. Lord, A., Kalimo, H., Eckman, C., Zhang, X.Q., Lannfelt, L. and Nilsson, L.N. (2006) The Arctic Alzheimer mutation facilitates early intraneuronal Abeta aggregation and senile plaque formation in transgenic mice. *Neurobiol. Aging*, **27**, 67–77.
58. Oakley, H., Cole, S.L., Logan, S., Maus, E., Shao, P., Craft, J., Guillozet-Bongaarts, A., Ohno, M., Disterhoft, J., Van Eldik, L. *et al.* (2006) Intraneuronal beta-amyloid aggregates, neurodegeneration, and neuron loss in transgenic mice with five familial Alzheimer's disease mutations: potential factors in amyloid plaque formation. *J. Neurosci.*, **26**, 10129–10140.
59. Oddo, S., Caccamo, A., Shepherd, J.D., Murphy, M.P., Golde, T.E., Kayed, R., Metherate, R., Mattson, M.P., Akbari, Y. and LaFerla, F.M. (2003) Triple-transgenic model of Alzheimer's disease with plaques and tangles: intracellular Abeta and synaptic dysfunction. *Neuron*, **39**, 409–421.
60. Wirths, O., Multhaup, G., Czech, C., Blanchard, V., Moussaoui, S., Tremp, G., Pradier, L., Beyreuther, K. and Bayer, T.A. (2001) Intraneuronal Abeta accumulation precedes plaque formation in beta-amyloid precursor protein and presenilin-1 double-transgenic mice. *Neurosci. Lett.*, **306**, 116–120.
61. Gouras, G.K., Tsai, J., Naslund, J., Vincent, B., Edgar, M., Checler, F., Greenfield, J.P., Haroutunian, V., Buxbaum, J.D., Xu, H. *et al.* (2000) Intraneuronal Abeta42 accumulation in human brain. *Am. J. Pathol.*, **156**, 15–20.
62. Bahr, B.A., Hoffman, K.B., Yang, A.J., Hess, U.S., Glabe, C.G. and Lynch, G. (1998) Amyloid beta protein is internalized selectively by hippocampal field CA1 and causes neurons to accumulate amyloidogenic carboxyterminal fragments of the amyloid precursor protein. *J. Comp. Neurol.*, **397**, 139–147.
63. D'Andrea, M.R., Nagele, R.G., Wang, H.Y., Peterson, P.A. and Lee, D.H. (2001) Evidence that neurones accumulating amyloid can undergo lysis to form amyloid plaques in Alzheimer's disease. *Histopathology*, **38**, 120–134.
64. Oddo, S., Billings, L., Kesslak, J.P., Cribbs, D.H. and LaFerla, F.M. (2004) Abeta immunotherapy leads to clearance of early, but not late, hyperphosphorylated tau aggregates via the proteasome. *Neuron*, **43**, 321–332.
65. Manczak, M., Anekonda, T.S., Henson, E., Park, B.S., Quinn, J. and Reddy, P.H. (2006) Mitochondria are a direct site of A beta accumulation in Alzheimer's disease neurons: implications for free radical generation and oxidative damage in disease progression. *Hum. Mol. Genet.*, **15**, 1437–1449.
66. Caspersen, C., Wang, N., Yao, J., Sosunov, A., Chen, X., Lustbader, J.W., Xu, H.W., Stern, D., McKhann, G. and Yan, S.D. (2005) Mitochondrial Abeta: a potential focal point for neuronal metabolic dysfunction in Alzheimer's disease. *FASEB J.*, **19**, 2040–2041.
67. Ferreira, I.L., Resende, R., Ferreiro, E., Rego, A.C. and Pereira, C.F. (2010) Multiple defects in energy metabolism in Alzheimer's disease. *Curr. Drug Targets*, **11**, 193–206.
68. Billings, L.M., Oddo, S., Green, K.N., McGaugh, J.L. and LaFerla, F.M. (2005) Intraneuronal Abeta causes the onset of early Alzheimer's disease-related cognitive deficits in transgenic mice. *Neuron*, **45**, 675–688.
69. Morris, R.G., Anderson, E., Lynch, G.S. and Baudry, M. (1986) Selective impairment of learning and blockade of long-term potentiation by an N-methyl-D-aspartate receptor antagonist, AP5. *Nature*, **319**, 774–776.
70. Gong, B., Cao, Z., Zheng, P., Vitolo, O.V., Liu, S., Staniszewski, A., Moolman, D., Zhang, H., Shelanski, M. and Arancio, O. (2006) Ubiquitin hydrolase Uch-L1 rescues beta-amyloid-induced decreases in synaptic function and contextual memory. *Cell*, **126**, 775–788.
71. Marjanska, M., Curran, G.L., Wengenack, T.M., Henry, P.G., Bliss, R.L., Poduslo, J.F., Jack, C.R. Jr, Ugurbil, K. and Garwood, M. (2005) Monitoring disease progression in transgenic mouse models of Alzheimer's disease with proton magnetic resonance spectroscopy. *Proc. Natl Acad. Sci. USA*, **102**, 11906–11910.
72. Oberg, J., Spenger, C., Wang, F.H., Andersson, A., Westman, E., Skoglund, P., Sunnemark, D., Norinder, U., Klason, T., Wahlund, L.O. *et al.* (2008) Age related changes in brain metabolites observed by 1H MRS in APP/PS1 mice. *Neurobiol. Aging*, **29**, 1423–1433.
73. Palop, J.J. and Mucke, L. (2010) Amyloid-beta-induced neuronal dysfunction in Alzheimer's disease: from synapses toward neural networks. *Nat. Neurosci.*, **13**, 812–818.
74. Hassel, B., Johannessen, C.U., Sonnewald, U. and Fonnum, F. (1998) Quantification of the GABA shunt and the importance of the GABA shunt versus the 2-oxoglutarate dehydrogenase pathway in GABAergic neurons. *J. Neurochem.*, **71**, 1511–1518.
75. Morita, M., Al-Chalabi, A., Andersen, P.M., Hosler, B., Sapp, P., Englund, E., Mitchell, J.E., Habgood, J.J., de Belleroche, J., Xi, J. *et al.* (2006) A locus on chromosome 9p confers susceptibility to ALS and frontotemporal dementia. *Neurology*, **66**, 839–844.